Biodistribution and inflammatory response of intracranial delivery of scintillating nanoparticles

Máté Fischer[1], Amber Zimmerman[1], Eric Zhang[3], Joseph Kolis[3], Ashley Dickey[3], Mary K. Burdette[3], Mitra Afaghpour-Becklund[1], Praveen Chander[1], Stephen H. Foulger[3,4,5], Jonathan L. Brigman[1,2], & Jason. P. Weick[1,2]

[1]Department of Neurosciences
[2]Center for Brain Recovery and Repair
University of New Mexico HSC
Albuquerque, NM 87131, USA.

[3]Department of Materials Science and Engineering
[4]Center for Optical Materials Science and Engineering Technologies
[5]Department of Bioengineering
Clemson University, Clemson, SC 29634-0971, USA

Running Title: Inorganic Scintillators and Circuit Function

Number of Words in Abstract: 350

Number of Words in Manuscript: 5222

Number of Figures: 7

Keywords: radioluminescent, scintillator, optogenetics, biocompatible, LTP, YSO:Ce

*Corresponding Authors:

This project was supported by an NSF EPSCoR track II award (NSF1632881)

Abbreviated title:
Figures: X, Pages: XX, Abstract words: XX, Introduction words: XX, Discussion words: XX, Supplemental Material Files: X

Abstract

Nanoparticle-based delivery systems have become a popular method for targeting tumors and impermeable tissue with drugs for treatment and imaging markers for biodetection. Nanomaterials are beneficial for medical treatment because they can be modified to have increased stability and carrying capacity, and their size and surface modifications allow them to reach otherwise impenetrable tissue. Nanoparticles have become particularly popular in medical imaging since they can be produced as scintillators that emit visible light which can be used in PET detectors, or they could be made with paramagnetic materials for magnetic resonance imaging. Localized or systemic injection can be used for delivery of nanoparticles; however, systemic injection without appropriate surface modifications is subjected to uptake by the mononuclear phagocytic system which clears particles from the circulation rapidly limiting their accumulation at target tissue and reducing efficacy. Here we demonstrate the biodistribution of Yttrium oxyorthosilicate nanoparticles doped with Cerium after localized injection to the cerebral cortex.

Introduction

Nanoparticles have become an increasingly popular tool for many applications ranging from diagnostics to drug delivery and targeted therapies (Soppimath 2001, Faraji 2009, Bahrami 2017). Much research has gone into the development of nanomaterials that are biocompatible and do not elicit a deleterious immune response. Despite this enormous promise of this emerging technology, issues with the delivery, targeting, toxicity and clearance of nanoparticle-based drug delivery systems leave many unresolved questions (Longmire 2008, Ray 2009). One strategy currently in development is to modify the surface chemistries of nanoparticles in such a way as to address these concerns, aiming to alter particles in ways that promote stability and minimize toxicity (Kango 2013).

In addition to modifying surface chemistries, researchers have also taken advantage of the fact that nanoparticles generated from different starting materials also display an enormous amount of variability in their biocompatibility and utility (Faraji 2009). Silicon-based nanoparticles have been especially extensively probed for potential medical applications due to their low inherent toxicity, especially when administered chronically (Murugadoss 2017). Wide band gap materials doped with rare earth ions are under intense research for their applications in medical imaging and have been used in the development of PET detectors for their scintillating properties (Loudyi 2007). More recently however, rare earth orthosilicates such as Yttrium orthosilicate doped with cerium Y_2SiO_5:Ce (YSO:Ce) have been studied for their additional scintillating properties (Ricci 2008, Hamroun 2018). Scintillating nanoparticles provide a popular platform for biomedical applications because of their ability to produce light upon stimulation that can be detected through different imaging modalities. Scintillators such as YSO:Ce allow investigators to deliver specific spectra of light to targeted areas that can be for applications such as optogenetic manipulations (Melcher 2000, Pignalosa 2012). YSO:Ce's specific blue light emission spectrum,

typically used in LEDs and phosphors, might provide a novel light delivery method to the brain with minimal light scatter (Krämer 2003, Gonzales-Ortega 2005).

Currently, *in vivo* optogenetic methods require an implantable optical fiber into a target region containing a bacterial opsin consisting of a channel that is capable of excitation following stimulation with specific wavelengths (Cardin 2010). Scintillating nanoparticles could be developed to emit a variety of spectra that could be used to replace these optical fibers. Cell type-specific expression of optically-activated constructs paired with light stimulation from localized scintillating nanoparticles would provide a far less invasive platform for optogenetics than current available methods of intracranial light delivery such as surgical implantation of optical fibers. Previous work has demonstrated that only a median of 0.7% of systemically injected nanoparticles passively reached their target tissue, which limits the efficacy of these particles to nearly zero (Wilhelm 2016). Recent research suggests that nanoparticle therapy would be most beneficial if organs are targeted locally rather than systemically to avoid loss of particles to the mononuclear phagocytic system (Wei 2018). Intracranial injection of nanoparticles to a target region would bypass the mononuclear phagocytic system and allow for specific localization of particles to a brain region of interest. Additionally, nanoparticles can be designed with surface modifications that tether them in close proximity to their sensors to provide more directed light stimulation in a cell-specific manner and increase their chemical stability.

However, little is currently known regarding the biodistribution or toxicity of scintillating particles delivered via intracranial injection. In the current study, we examined the biodistribution of and inflammatory response mounted against scintillating nanoparticles delivered into mouse cortex in order to determine the feasibility and efficacy of utilizing these particles for *in vivo* stimulation in future studies. C57BL/6J mice were given intracranial delivery of YSO-BSA-Fluorescein nanoparticles at differing concentrations targeting premotor cortex (M2) as it is a commonly targeted area in optogenetic experiments. Follow infusion, we examined the

distribution and neuro inflammatory response was measured each at specific post-infusion time points.

Methods:

Synthesis of Yttrium orthosilicate nanoparticles

Sub 100 nm silica cores were synthesized by the sol-gel process with 27 mmol (6.0 mL) of tetra ethyorthosilicate, 167 mmol (3 mL) of water, and 50 mmol (2 mL) of ammonia hydroxide (28% v/v) in 150 mL of ethanol at room temperature under vigorous stirring condition for 20 hrs. The particles were then washed with ethanol (2x) and water (1x). Silica (120 mg) was disperse in water (100 mL) with 1.98 mmol (760 mg) of yttrium nitrate hexahydrate and 15 µmol (6.5 mg) of cerium nitrate hexahydrate. Ammonia hydroxide (1 mL) was added drop wise into the solution and vigorously stirred for 16 hrs in room temperature. The waters were washed with water (3x) and dried at 125OC. The particles were annealed at 1000oC for 1 hr.

Characterization of core-shell yttrium orthosilicate nanoparticles

Sub 100 nm particulates were dispersed in water on double-sided carbon tape and mounted onto a scanning electron microscope stub. The particles were plasma coated with platinum. A Hitachi 4800 scanning electron microscope was used to image the particles at 20 kV and 10 mA. Photoluminescence and excitation measurements were taken by a Jobin Yvon Fluorolog 3-222 spectrometer with a pump source of 360 nm. X-ray luminescence was measured with a Horiba JY synapse CCD camera, Horiba JY microHR monochromator, and a tungsten target Amptek mini x-ray source at 40 kV and 99 µA.

Experimental subjects

Female C57BL/6J mice (The Jackson Laboratory, Bar Harbor, ME) were housed in a temperature- and humidity- controlled vivarium under a reverse 12 h light/dark cycle (lights off 0800 h). All experimental procedures were performed in accordance with the National Institutes of Health Guide for Care and Use of Laboratory Animals and were approved by the University of New Mexico Health Sciences Center Institutional Animal Care and Use Committee.

Microinjection of Nanoparticles

At approximately 6 months of age, mice were anesthetized with isoflurane and fixed in a stereotaxic apparatus (1900 Stereotaxic Alignment System, David Kopf Instruments, Tujunga, CA) as previously described (Brigman & Josey 2015, Marquardt 2019). A 33-gauge infusion cannula (Plastics One, Roanoke, VA) attached with polyurethane tubing to a Hamilton syringe (Hamilton, Reno NV) was directed at secondary motor cortex (M2. AP: 1.345, ML: +/- 0.6, DV: -1.0). YSO-BSA-Fluorescein nanoparticles (0.5 µl) saline vehicle was infused over 5 min using a pump (GenieTouch, Kent Scientific, Torrington, CT), with the cannula left in place for an additional 2.5 min to allow full diffusion. Mice were inject with 1mg/ml and 3mg/ml in contralateral hemispheres. On completion of the last infusion, mice were sutured and returned to their home cages.

Immunohistochemistry

At 24, 72 or 216 hours (9 days) post-injection, mice were sacrificed by cervical dislocation, brains extracted and placed in 4% paraformaldehyde solution for 24 hours. 50 µm coronal sections were cut with a vibratome (Classic 1000 model, Vibratome, Bannockburn, IL) adjacent to the site of injection. Slices were blocked and permeabilized for 1 hour on a Belly Dancer shaking platform (IBI Scientific) in a 500µL solution of 10% donkey serum, and 0.5% Triton X-100, brought to volume with 1x PBS. After one hour incubation at room temperature the blocking solution was removed and replaced with 500µL of primary antibody solution containing monoclonal mouse anti-GFAP (dilution: 1:500; Neuromab, USA) and polyclonal rabbit anti-Iba-1 (dilution: 1:250; Wako, Japan) diluted in 5% donkey serum and 0.25% Triton X-100 brought to volume in PBS. Sections were covered and incubated in a 4˚C walk-in cold room overnight. The following day, the primary antibody solution was removed and slices were washed 3 times with 500µL PBS for 5 minutes each. Following the three washes, 500µL of secondary antibody solution containing donkey anti-mouse AlexaFluor 647 (dilution: 1:500; Abcam, USA) and donkey anti-rabbit AlexaFluor 550 (dilution: 1:500; Abcam, USA) diluted in 5% donkey serum and 0.25% Triton X-100 brought to

volume in PBS was added to the sections at room temperature for 1 hour. After this incubation the secondary antibody solution was removed and slices were washed 3 times with 500 µL 1xPBS for 5 minutes each. DAPI counterstaining (1:10000 concentration in PBS) was then performed and slices were placed on a rocker for 10 minutes shielded from light. Finally, the slices were washed 3 times with 500µL PBS for 5 minutes each and mounted to glass microscope slides. Slices were covered with 100µL of Fluoromount-G (Thermo Fischer Scientific, USA) and then sealed with glass coverslips, making sure to remove any air bubbles. Slides were finally stored in a 4˚C refrigerator for subsequent imaging.

Confocal Microscopy

Following immunostaining and mounting, fluorescence-tagged immune cell populations were counted using a Leica TCS SP8 Confocal Microscope (Leica Microsystems). DAPI, nanoparticle-conjugated FITC and secondary antibody-conjugated fluorophores were excited using a 405nm laser diode and a tunable pulse white light laser respectively with a 63x oil immersion objective and captured using hybrid spectral detectors (HyD). Zstacks were then collected with a Z-range of 70um. Z stacks of adjacent slices were ordered and merged to estimate the extent of the nanoparticle spread and compressed then into a two dimensional image using the maximal intensity projection algorithm in the Leica LASX software package. Maximum projection maps were exported as uncompressed TIFF files and transferred to ImageJ image analysis software.

Analysis and Statistics

Optical sections of 25um thickness were collected for the brains that were sectioned and stained for quantification of NP, Iba-1 and Gfap signals, respectively. After Z stacks were compressed, ImageJ software was used to draw regions of interest (ROIs) surrounding the entire extent of the M2 region as represented by the Allen Brain Atlas for the given appropriate A/P range. Light signal from photon scatter around the edges of tissue, tears in the tissue as wells as vasculature were excluded from analysis. Mean fluorescence intensities were calculated over the ROIs, and a

background measurement taken from cortical regions outside M2 was subtracted from these values. A ratio was then calculated for signal intensity in the NP vs. vehicle treated hemispheres and mean values with SEM were reported for each time point. ImageJ was also scaled so that the pixel to mm ratio was defined for each image and using this scale, the area of the extent of NP spread was calculated by manually tracing the outlines of the FITC signal adjacent to the site of injection.

Results:

To determine the extent of spread of injected nanoparticles, animals that received the particles were sacrificed 24hr, 48hr and 9 days post injection and the FITC fluorophore conjugated to the nanoparticles was imaged across the extent of the M2 region. Confocal imaging of the region surrounding the injection site revealed reliably detectable FITC in non-perfused animals (Figure 3A, D), but no detectable signal in animals that were perfused with 4% PFA upon sacrifice. In the non-perfused groups 50um slices were immunostained for the astrocytic marker Gfap as well as the microglial marker Iba-1 for subsequent analyses (Figure 3B, E). Due to light scatter in the sample along edges and tears in the tissue, as well as vasculature also giving off fluorescent signal, care was taken to exclude these confounds from analysis (Figure 3C, D). With this in mind we set out to quantify the area and intensity of the spread of NPs as well as the presence of inflammatory cells in the M2 region.

To accomplish this quantification, Z stacks were collected across the extent of the M2-containing brain sections and stacks were reconstructed with Leica LASX software (Figure 4A). Based on this 3D reconstruction it was determined that the injected NPs spread to fill an area of approximately 0.091mm^3 in the 24hr group, 0.097mm^3 in the 48hr group and just 0.0101mm^3 in the long term group (Figure 4B). The drop in signal intensity adjacent to the injection site between the 72 hour and 9 day time points could indicate either an active clearance of the particles to the lymphatic system or a passive diffusion of the particles through the M2 region away from the injury site between those two time points. To address this, Z stacks were then flattened according to a maximal intensity projection algorithm and ImageJ software was utilized to measure mean fluorescence intensity for the NP-FITC signaling across the entire extent of the M2 region from both the NP injected (ipsilateral) and vehicle-injected (contralateral) sides. These fluorescence measurements were normalized to a cortical background level outside the M2 region and are shown as a ratio of the intensity of the FITC signal in hemisphere ipsilateral to the injection over

the contralateral side (Figure 4C). Interestingly, while the size of the bright NP-FITC signal adjacent to the injection site diminished notably by the 9 day time point, no difference was established in the overall mean fluorescence intensity across M2 in the same time frame, indicating the persistence of NPs in the M2 region, likely due to passive diffusion from the site rather than clearance from the tissue overall.

As mentioned, brain sections were stained with antibodies against astrocyte marker Gfap as well as microglial marker Iba-1 near the injection site to determine whether or not the brain immune system mounted an inflammatory response to the presence of the particles. Representative images for each the Iba-1 (Figure 5A) and the Gfap (Figure 5B) staining, respectively, show that both glial cell types were readily detectable in the mouse gray matter. Maximal projection maps were again generated for the region of interest and mean fluorescence intensities over the M2 region were determined for each time point. According to these quantifications, Iba-1 intensity is significantly increased between 24 hours post-injection transiently ($p=0.0375$) and then returns to baseline levels by the latter time point ($p=0.0475$) (Figure 5C). Presence of $Gfap^+$ astrocytes also showed temporal regulation following NP injection, but in this case demonstrated maximal response 24 hours following the particle delivery, only to return to baseline levels by the 72 hour mark ($p<0.001$) and stay low at the 9 day time point ($p<0.001$) (Figure 5D).

While our data do suggest that an immune response is mounted against the particles that is greater in magnitude than that of our control saline injection, it seems that after 9 days in the brain, any inflammatory response has been normalized and the particles not only diffuse passively from the site of injection, but remain in the brain to an extent indistinguishable from merely 24 hours after the NPs are delivered. These findings taken together suggest a potential utility for injectable YSO:Ce nanoparticle platform in the delivery of light or any surface modified residue to brain tissue with a minimal, transient induction of neuroinflammation that may be superior to long-

term surgical interventions currently required for optogenetic, electrode arrays and other applications for probing murine neural function and networks.

Discussion:

The use of nanoparticles for optogenetic modulation of neuronal function is supported by several current studies. From drug and gene delivery to imaging to optical stimulation, nanoparticles could serve as a platform technology for a new wave of medical and research initiatives (Singh 2011). For instance, Bartely and colleagues observed that light emitted from LSO:Ce microparticles in response to UV stimulation caused an increase in the frequency of sEPSCs onto CA1 pyramidal cells expressing ChR2. Inherent properties of the particles such as photon emission by scintillation as well as diverse modifications to surface chemistry can be readily achieved, making the biological compatibility of such particles the next major hurdle for most preclinical and clinical research (Ai 2011). However, Bartley *et al.* were not able to detect firing of action potentials or large light-evoked EPSCs, consistent with the relatively small photocurrents observed. In this report, we surface labeled scintillating YSO:Ce nanoparticles with a FITC fluorophore and injected these particles into the M2 region of mouse cerebral cortex. These particles were applied to the surface of acute slice preparations, with estimated distance from recorded ChR2-expressing cells of 100 microns or more (Bartely et al., in press). 24 hours, 72 hours and 9 days post-injection mice were sacrificed and their M2 regions were assayed on the NPO-injected and vehicle-treated side to probe the spread of particles and the inflammatory response mounted to the particles. Overall, we found that particles persisted through the 9-day post-injection time point, but some time after 72 hours the particles diffused away from the site of the injection while remaining in the M2 cortical region. Thus, our results support the notion that direct injection of particles could be used prior to slice preparation to directly test for greater ChR2 activation due to closer proximity and reduced light attenuation from scattering (REF). Some work has been done concerning the diffusion dynamics of nanoparticles in vitro, but wide variation in

nanoparticle size, composition, surface chemistry, injection load and target tissue yield a wide heterogeneity of results (REF). The particles synthesized and utilized in this paper however yield promising preliminary results for the diffusibility of the particles though gray matter. This begs the follow-up question of to what degree exactly is the local microenvironment and relevant inflammatory factors will tolerate the injected material. To this end we assayed the recruitment of Iba-1 expressing microglia and Gfap-expressing

The study by Bartely et al., (in press) also observed no inflammatory response of LSO:Ce microparticle exposure in acute hippocampal slices as assessed by GFAP staining. However, while our results don't preclude an effect prior to 24 hours, we did see significantly increased GFAP expression present in brain regions that received particle injections at 24 hr, but not in control hemispheres. The delayed IBA1 expression observed at 72 hours suggest that the inflammatory response takes time to develop in response to particle injection. Furthermore, Bartely and colleagues did observe small changes in synaptic function including a small reduction in the frequency of excitatory postsynaptic currents (EPSCs) and an increase in paired pulse ratio of evoked excitatory transmission, indicating an effect of the particles on presynaptic release probability (Dobrunz and Stevens, 1997). Alterations in neuronal excitability have been shown to modulate presynaptic release probability (Crabtree et al., 2017), suggesting that this could be the underlying mechanism for the minor effects on synaptic function with application of the LSO:Ce microparticles. These effects are likely independent of inflammatory changes that can also alter synaptic function (REF). In addition, while LSO:Ce particles should act similarly on surrounding tissue due to surface chemistry, there remains a possibility that the YSO:Ce particles used in the current study may act differently within the brain. Thus, future studies are needed to determine whether injected YSO:Ce particles have the same or different effects on neurotransmission.

Figures:

Figure 1 – Chemical Preparation of Nanoparticles

a. Synthesis of YSO nanoparticles
b. Schematic of scintillation
c. Electron micrograph of particles
d. Spectral characterization of NPs

Figure 2 – Injection Details and Experimental Design

a. Timeline of experiments
b. Photograph of stereotax/injection apparatus
c. Stereotaxic information/brain map

Figure 3 – Representative Images of staining and injection site

a. NPs and DAPI full brain
b. Iba-1 and Gfap full brain
c. Merge brain merge with inset
d. Inset NPs and DAPI
e. Inset Iba-1 and GFAP
f. Inset full merge

Figure 4 – Spread of NPs

a. 3D render of slice
b. Volume of spread
c. Fluorescence intensity time course

Figure 5 – Neuroinflammatory Response

a. Representative Iba-1 stain
b. Representative Gfap stain
c. Iba-1 MFI time course
d. Gfap MFI time course

Figure 1

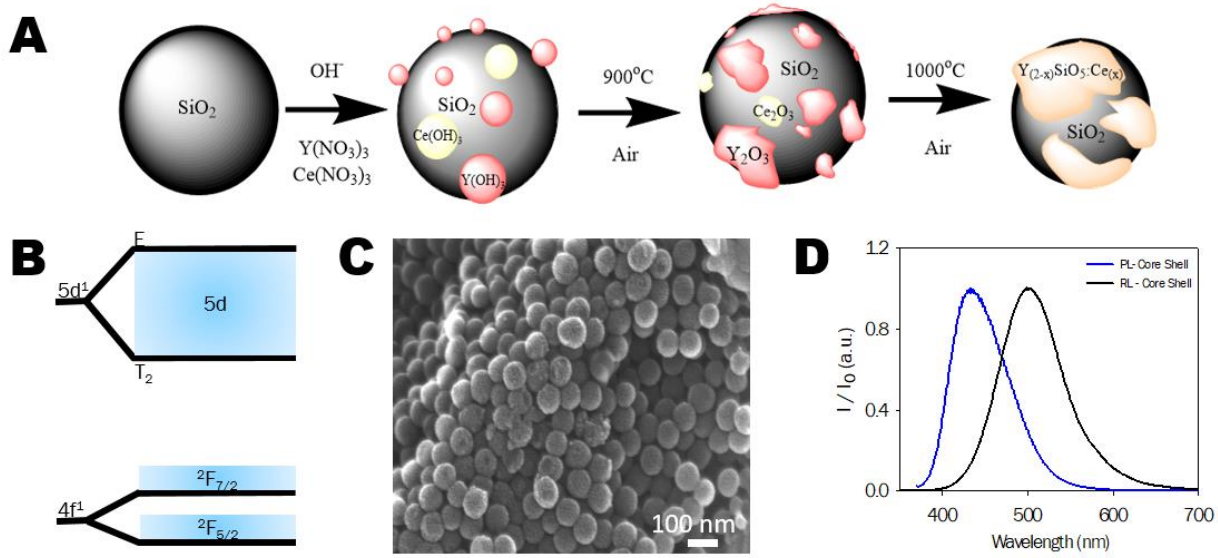

A) Schematic of the development of YSO:Ce using a core-shell method.
B) Relaxation of cerium from it higher energy 5d state to its respective ground state of $^2F_{7/2}$ and $^2F_{5/2}$ in the Ce 1 site.
C) SEM of NPs synthesized by the core-shell method.
D) Photoluminescence and radioluminescence of nano core shell particulates irradiated by 360 nm and a broadband 40 KeV tungsten x-ray source, respectively.

Figure 2

Figure 3

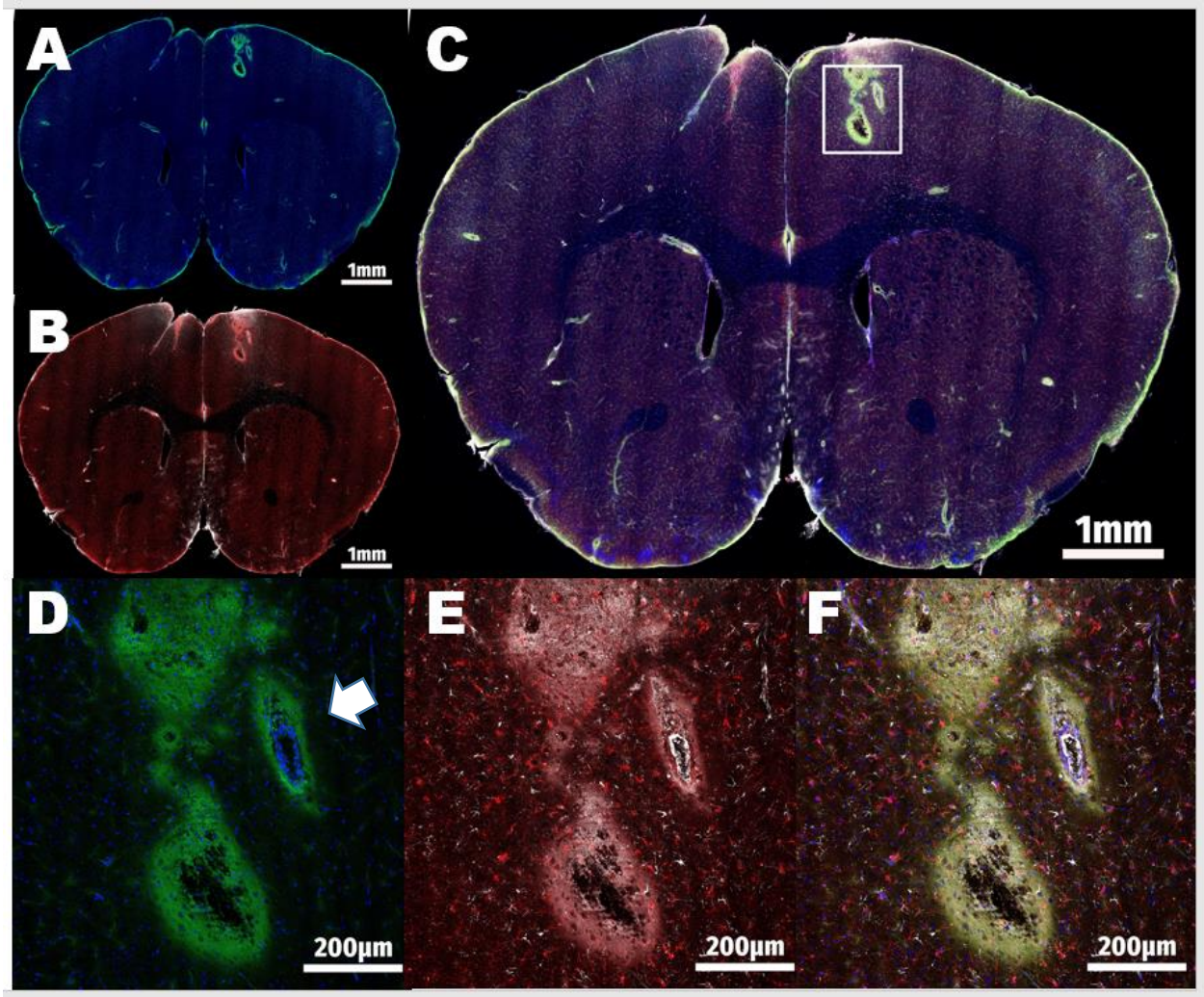

A) Full 40x tile scan of NP-injected mouse brain showing NP-FITC in green and nuclear DAPI staining in blue. The green signal around the edges of the tissue due to light scatter was excluded from analysis

B) Same mouse brain showing Iba-1 (red) staining as well as Gfap (white)

C) Merge of NPs (green), DAPI (blue), Iba-1 (red) and Gfap (white) staining as well as highlighting area of inset shown in D-F

D) NP and DAPI staining show in 63x tiled insert. White arrow is indicating a blood vessel excluded from analysis

E) Regularly distributed Iba-1-expressing (red) microglia are clearly visible at higher magnification as well as Gfap-expressing (white) astrocytes

F) 4 channel merge demonstrates the area of extent of RLP spread as well as the presence of neural immune cells

Figure 4

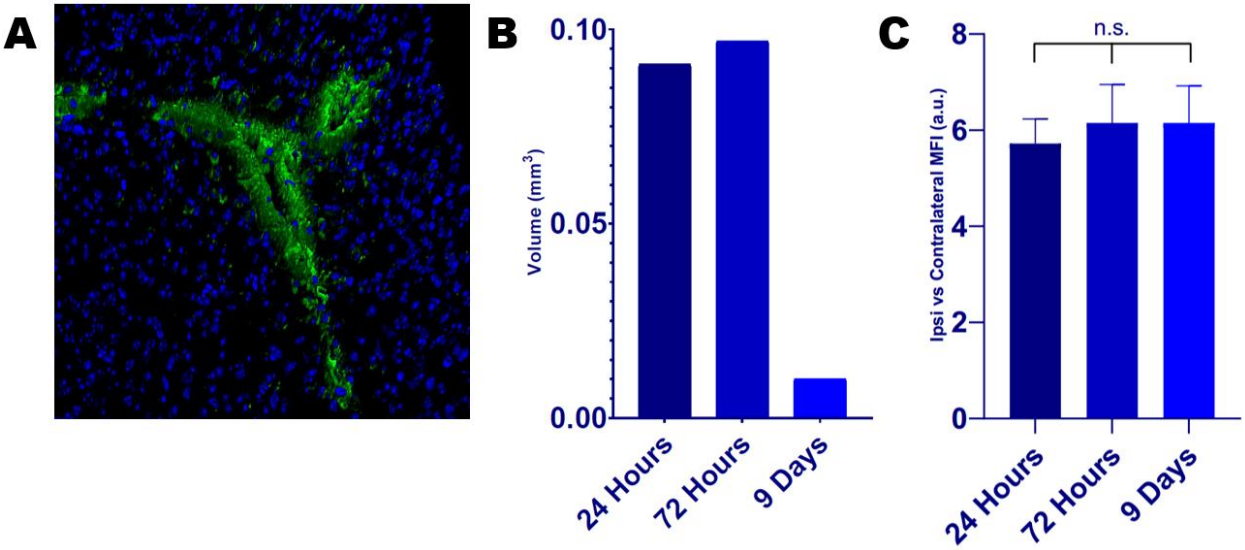

A) 3D render of an injection site, representative of the analysis used to approximate the spread of NPs from the M2 injection site

B) Time course of the area of extent of bright NP signal adjacent to the injection site shows no change across the first 72 hours, but a sharp decline at 9 days, indicating diffusion or clearance from the injury site in that time

C) Interestingly, the ratio of NP fluorescence of the ipsi- to contralateral side remained unchanged over the 9 days assayed, suggesting the persistent presence of NPs despite the diffusion from the injection site

Figure 5

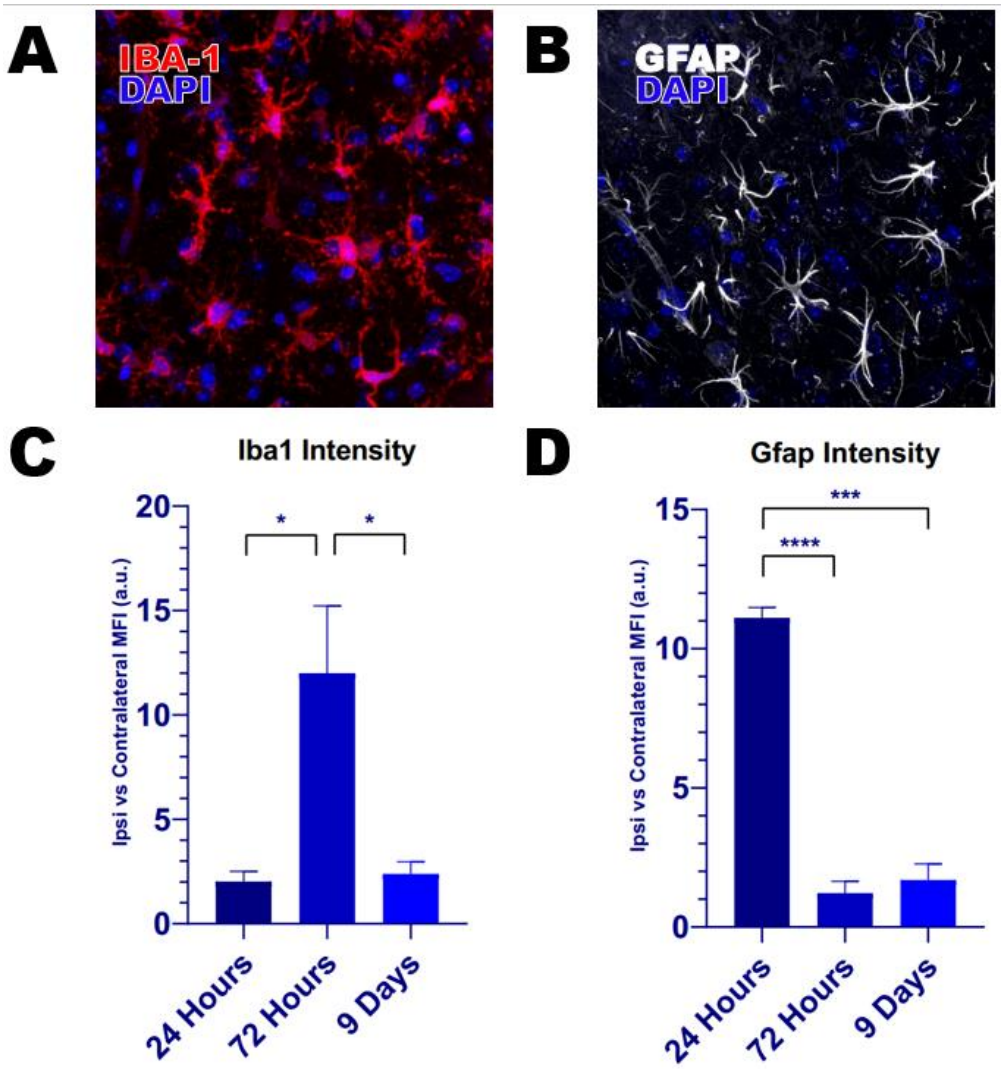

A) Representative image of Iba-1 staining for microglia

B) Representative image of Gfap staining for astrocytes

C) Time course of Iba-1 intensity shows an elevation in microglial staining across the entire M2 region at 72 hours post-injection, but not 24 hours or 9 days

D) Time course of Gfap intensity shows an elevation in astrocytic staining across the entire M2 region 24 hours post-injection, but not at later time points

References:

1. Aravanis AM, Wang L-P, Zhang F, Meltzer LA, Mogri MZ, Schneider MB, et al. An optical neural interface: in vivo control of rodent motor cortex with integrated fiberoptic and optogenetic technology. Journal of Neural Engineering. 2007 Sep 1;4(3):S143–56.

2. Wilhelm S, Tavares AJ, Dai Q, Ohta S, Audet J, Dvorak HF, et al. Analysis of nanoparticle delivery to tumours. Nature Reviews Materials [Internet]. 2016 May [cited 2019 Apr 2];1(5). Available from: http://www.nature.com/articles/natrevmats201614

3. Soppimath KS, Aminabhavi TM, Kulkarni AR, Rudzinski WE. Biodegradable polymeric nanoparticles as drug delivery devices. Journal of Controlled Release. 2001 Jan;70(1–2):1–20.

4. Ricci PC, Carbonaro CM, Chiriu D, Corpino R, Faedda N, Marceddu M, et al. Ce3+-doped lutetium yttrium orthosilicate crystals: Structural characterization. Materials Science and Engineering: B. 2008 Jan;146(1–3):2–6.

5. Longmire M, Choyke PL, Kobayashi H. Clearance properties of nano-sized particles and molecules as imaging agents: considerations and caveats. Nanomedicine. 2008 Oct;3(5):703–17.

6. Pignalosa P, Liu B, Chen H, Smith H, Yi Y. Giant light extraction enhancement of medical imaging scintillation materials using biologically inspired integrated nanostructures. Optics Letters. 2012 Jul 15;37(14):2808.

7. Krämer KW, Biner D, Frei G, Güdel HU, Hehlen MP, Lüthi SR. Hexagonal Sodium Yttrium Fluoride Based Green and Blue Emitting Upconversion Phosphors. Chemistry of Materials. 2004 Apr;16(7):1244–51.

8. Wei Q, Huang C, Zhang Y, Zhao T, Zhao P, Butler P, et al. Mechanotargeting: Mechanics-Dependent Cellular Uptake of Nanoparticles. Advanced Materials. 2018 Jul;30(27):1707464.

9. Bahrami B, Hojjat-Farsangi M, Mohammadi H, Anvari E, Ghalamfarsa G, Yousefi M, et al. Nanoparticles and targeted drug delivery in cancer therapy. Immunology Letters. 2017 Oct;190:64–83.

10. Bahrami B, Hojjat-Farsangi M, Mohammadi H, Anvari E, Ghalamfarsa G, Yousefi M, et al. Nanoparticles and targeted drug delivery in cancer therapy. Immunology Letters. 2017 Oct;190:64–83.

11. Faraji AH, Wipf P. Nanoparticles in cellular drug delivery. Bioorganic & Medicinal Chemistry. 2009 Apr;17(8):2950–62.

12. Lee SH, Kim J, Shin JH, Lee HE, Kang I-S, Gwak K, et al. Optogenetic control of body movements via flexible vertical light-emitting diodes on brain surface. Nano Energy. 2018 Feb;44:447–55.

13. Hamroun MSE, Guerbous L, Bensafi A. Photoluminescence spectroscopy and structural characterization of Ce3+-doped LYSO nanocrystalline powders. Optik. 2018 Apr;158:1548–52.

14. Melcher CL. Scintillation Crystals for PET. :6.

15. Kango S, Kalia S, Celli A, Njuguna J, Habibi Y, Kumar R. Surface modification of inorganic nanoparticles for development of organic–inorganic nanocomposites—A review. Progress in Polymer Science. 2013 Aug;38(8):1232–61.

16. Cardin JA, Carlén M, Meletis K, Knoblich U, Zhang F, Deisseroth K, et al. Targeted optogenetic stimulation and recording of neurons in vivo using cell-type-specific expression of Channelrhodopsin-2. Nature Protocols. 2010 Feb;5(2):247–54.

17. Ray PC, Yu H, Fu PP. Toxicity and Environmental Risks of Nanomaterials: Challenges and Future Needs. Journal of Environmental Science and Health, Part C. 2009 Feb 17;27(1):1–35.

18. Murugadoss S, Lison D, Godderis L, Van Den Brule S, Mast J, Brassinne F, et al. Toxicology of silica nanoparticles: an update. Archives of Toxicology. 2017 Sep;91(9):2967–3010.

19. Loudyi H, Guyot Y, Gâcon J-C, Pédrini C, Joubert M-F. Understanding the scintillation efficiency of cerium-doped LSO, LYSO, YSO and LPS crystals from microwave study of photoconductivity and trapping. Optical Materials. 2007 Sep;30(1):26–9.

20. Gonzalez-Ortega JA, Tejeda EM, Perea N, Hirata GA, Bosze EJ, McKittrick J. White light emission from rare earth activated yttrium silicate nanocrystalline powders and thin films. Optical Materials. 2005 Apr;27(7):1221–7.